ACS APPLIED MATERIALS & INTERFACES

www.acsami.org

Surface Passivation of Efficient Nanotextured Black Silicon Solar Cells Using Thermal Atomic Layer Deposition

Wei-Cheng Wang,[†] Che-Wei Lin,[†] Hsin-Jui Chen,[†] Che-Wei Chang,[†] Jhih-Jie Huang,[†] Ming-Jui Yang,[‡] Budi Tjahjono,[‡] Jian-Jia Huang,[§] Wen-Ching Hsu,[§] and Miin-Jang Chen*,[†,∥]

[†]Department of Materials Science and Engineering, National Taiwan University, Taipei 106, Taiwan

[‡]Sunrise Global Solar Energy Co., Ltd., Yilan 268, Taiwan

[§]Sino-American Silicon Products Inc., Hsinchu Science Park 30075, Taiwan

[∥]Taiwan National Nano Device Laboratories, Hsinchu 30078, Taiwan

ABSTRACT: Efficient nanotextured black silicon solar cells passivated by an Al_2O_3 layer are demonstrated. The broadband antireflection of the nanotextured black silicon solar cells was provided by fabricating vertically aligned silicon nanowire (SiNW) arrays on the n^+ emitter. A highly conformal Al_2O_3 layer was deposited upon the SiNW arrays by the thermal atomic layer deposition (ALD) based on the multiple pulses scheme. The nanotextured black silicon wafer covered with the Al_2O_3 layer exhibited a low total reflectance of ~1.5% in a broad spectrum from 400 to 800 nm. The Al_2O_3 passivation layer also contributes to the suppressed surface recombination, which was explored in terms of the chemical and field-effect passivation effects. An 8% increment of short-circuit current density and 10.3% enhancement of efficiency were achieved due to the ALD Al_2O_3 surface passivation and forming gas annealing. A high efficiency up to 18.2% was realized in the ALD Al_2O_3-passivated nanotextured black silicon solar cells.

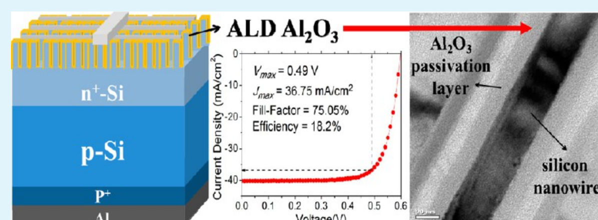

KEYWORDS: *nanotextured black silicon, solar cell, silicon nanowire, surface passivation, atomic layer deposition, aluminum oxide (Al_2O_3)*

INTRODUCTION

Antireflection (AR) is well known to be very important for the improvement of solar cell efficiency. The most popular AR technique used in silicon solar cells is the randomly distributed pyramids fabricated by anisotropic etching, together with a silicon nitride (SiN_x) film as the AR coating layer. However, such a structure is limited by small AR bandwidth and acceptance angles, which stimulates the development of other AR techniques. Recently, silicon nanowire (SiNW) arrays, also known as "black silicon", have attracted much attention because of the low reflectance over a broad range of incident wavelengths and angles.[1−9] A very low relative effective reflectivity (0.17%) has been achieved across a wide spectral range from 300 to 1000 nm, as demonstrated by Lu et al.[10] Many techniques, such as photo-lithographically defined etching,[1] reactive ion etching,[2−5] wet chemical etching,[6−8] and porous-Si etching,[11,12] had been proposed for preparing nanotextured black silicon. Among these techniques, silver-catalyzed wet chemical etching is a simple, cost-effective, and applicable approach.[7,8,10] However, a lot of defects are created at the surface of SiNWs during the fabrication process of SiNWs, resulting in remarkable surface recombination. Accordingly, the efficiency of nanotextured black silicon solar cells was typically much lower than that of conventional silicon solar cells.[13,14]

It is known that surface recombination is detrimental for many electrical and photonic devices, including silicon solar cells and light-emitting diodes.[3,15] Suppression of surface recombination has become essential due to the tendency toward the use of thinner crystalline silicon wafers.[16] Oh et al. used the tetramethylammonium hydroxide (TMAH) etch to control the surface morphologies and areas of black silicon.[17] The surface and Auger recombinations were simultaneously reduced and an efficiency up to 18.2% could be achieved in the black silicon solar cell. Recently, Mariani et al. reported the in situ passivation treatment can dramatically improve the external quantum efficiency and total power conversion efficiency of the GaAs-based nanopillar-array solar cells.[18] Holm et al. also demonstrated that the surface passivation is of crucial importance to the GaAsP single-nanowire solar cells.[19] Surface recombination can be reduced by deposition of a surface passivation layer ascribed to the following mechanisms: (1) the decrease in interfacial state density, i.e., the so-called chemical passivation, and (2) the reduction in minority carrier concentration near the interface by the built-in electric field, which is referred to as field-effect passivation.[20] The built-in electric field can be established by the appropriate fixed charge in the surface passivation layer, giving rise to repelling of minority carriers away from the interface so as to lower the

Received: July 18, 2013
Accepted: September 12, 2013
Published: September 12, 2013

ACS Publications © 2013 American Chemical Society

dx.doi.org/10.1021/am402889k | ACS Appl. Mater. Interfaces 2013, 5, 9752−9759

surface recombination rate. There have been a number of investigations of Al_2O_3 surface passivation layers prepared by atomic layer deposition (ALD) on silicon solar cells,[3,20,21] which have been reviewed comprehensively in ref 22. The ALD technique offers many benefits, including precise and easy thickness control, excellent step coverage and conformality, low defect density, high uniformity over a large area, good reproducibility, and low deposition temperatures, as a result of the self-limiting and layer-by-layer growth. Repo et al. has indicated that the ALD Al_2O_3 passivation layer makes huge improvement in the surface passivation and light absorption of black silicon.[23] Otto et al. also demonstrated that the surface recombination velocity can be reduced significantly by the conformal Al_2O_3 layer by ALD.[3] Recently, the black silicon solar cell with an efficiency as high as 18.7% have been reported using Al_2O_3 for passivation.[24] It has been also reported that the Al_2O_3 surface passivation layer prepared by plasma-assisted ALD works quite well upon the p^+ emitter in the p^+ emitter/n-base silicon solar cells[25] and on the rear surface of the n^+ emitter/p-base structure.[26] Nevertheless, it is inappropriate to use plasma-assisted ALD to deposit a surface passivation layer on the SiNWs with high aspect ratio, because of the reduced step coverage due to the involvement of reactive species which not only conduct ALD reactions but also react on saturated surface sites in the plasma-assisted ALD process.[27]

In this paper, we report that the surface passivation prepared by ALD contributes to efficiency enhancement of nanotextured black silicon solar cells with an n^+ emitter/p base structure. Instead of plasma-assisted ALD, the thermal ALD technique based on the multiple pulses scheme was used to prepare the Al_2O_3 surface passivation layer with high conformality on the surface of SiNWs upon the n^+ emitter. The total reflectance of the nanotextured black silicon wafer was reduced by the Al_2O_3 surface passivation layer. The effects of chemical and field-effect passivation on SiNW arrays on the n^+ emitter were elucidated, based on the effective minority carrier lifetime, interfacial state density, and effective oxide charge density in the Al_2O_3 layers. The analyses suggest that the chemical passivarion based on the reduction in interfacial state density is more effective than the field-effect passivation built by the appropriate oxide charge. The short-circuit current density was significantly enhanced by the ALD Al_2O_3 surface passivation layer, and an efficiency up to 18.2% was accomplished in the nanotextured black silicon solar cells.

EXPERIMENTAL SECTION

SiNW arrays were fabricated on (100), Czochralski-grown, 0.5–3 Ω·cm, ~180 μm thick, p-type silicon wafers using the silver-catalyzed wet chemical etching.[7,8,10,13,14,28] Before the fabrication of SiNW arrays, the silicon wafers were cleaned subsequently with acetone, ethanol, DI (de-ionized) water, and Piranha solution (H_2SO_4:H_2O_2 = 4:1, 60 min) and then rinsed with DI water and dipped into BOE (buffer oxide etch). Afterwards the silicon wafer was immersed in the chemical solution (0.1 M $AgNO_3$:HF:H_2O_2:DI water = 0.2:4:1.6:8, 5 min) composed of HF, H_2O_2, and Ag^+ at room temperature to fabricate the SiNW arrays.[7] By adjusting the concentration of the chemical solution, the diameter and length of SiNWs can be controlled. Since the silver clusters were located in the valleys between the SiNWs after the chemical etching process, the wafer was rinsed into the silver etchant solution (NH_3OH:H_2O_2 = 3:1, 15 min) to remove silver clusters.[7] Then the sample was quickly rinsed in DI water and dried at room temperature.

Figure 1 shows the schematic structure of the nanotextured black silicon solar cell. The n^+ emitter was phosphorus doped using phosphorous oxychloride ($POCl_3$) as the dopant source at the temperature of 825 °C. Then the phosphosilicate glass layer was removed with diluted HF solution. After the diffusion process, the back metallization was carried out by the screen-printing technique, followed by firing at 850 °C to form the back surface field (BSF). Following the BSF process, Ni/Ag was deposited by thermal evaporation through a shadow mask as the front metal contact. Afterwards, an Al_2O_3 surface passivation layer was deposited at 200 °C using the thermal ALD (Savannah, Cambridge Nanotech) technique. Trimethyl-aluminum (TMA, $Al(CH_3)_3$) and H_2O vapor were the precursors for aluminum and oxygen. Because of the high aspect ratio of SiNWs, a multiple pulses scheme was used to improve the infiltration of the precursors into the deep structure of SiNWs, i.e., one ALD cycle consisted of four pulses for TMA and subsequent four H_2O pulses as shown schematically in Figure 2. During the ALD process, the TMA results in the methyl-terminated surface of SiNWs to a depth determined by the dose of the precursor pulse. This renders the surface sites near the top of SiNWs nonreactive to the following TMA pulse, and so the following TMA pulse can only be chemisorbed on the deeper surface of SiNWs. Accordingly, the precursors can infiltrate into the deeper structure by the multiple pulses scheme. After the multiple TMA pulses, the subsequent multiple H_2O pulses react with the TMA chemisorbed on the surface so that one complete Al_2O_3 ALD cycle is finished.[29] The deposition rate of Al_2O_3 was 1.1 Å per ALD cycle using this multiple pulses scheme. Finally, the specimens were treated by forming gas annealing (FGA, 5% H_2/95% N_2) at 400 °C to improve the efficiency.

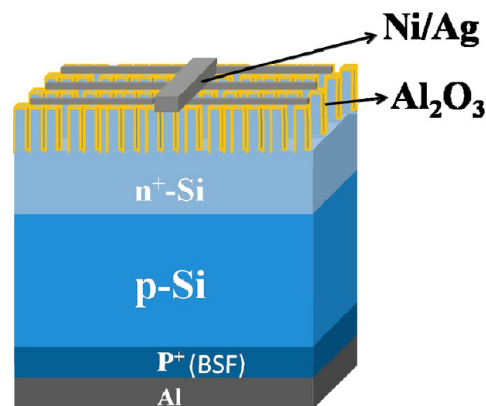

Figure 1. Schematic diagram of the nanotextured black silicon solar cell with an n^+ emitter/p base structure.

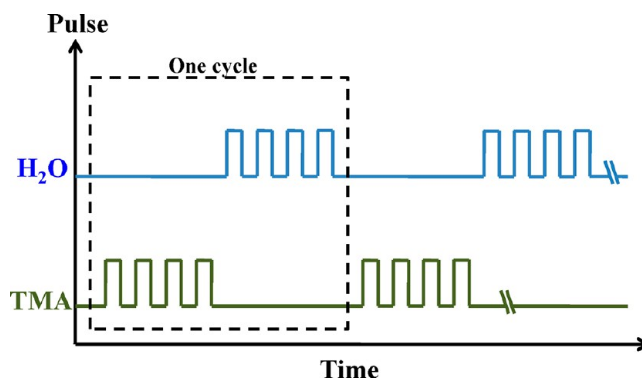

Figure 2. Multiple pulses scheme used in the ALD process.

The morphologies of SiNW arrays were characterized by scanning electron microscope (SEM) (Nova NanoSEM 450) and high-resolution transmission electron microscopy with energy dispersive spectrometer (HR-TEM with EDS, JEM-2100F Electron Microscope/JEOL Co. 200 KV). The total reflectance spectra of nanotextured black silicon wafers were measured by spectrophotometer in the

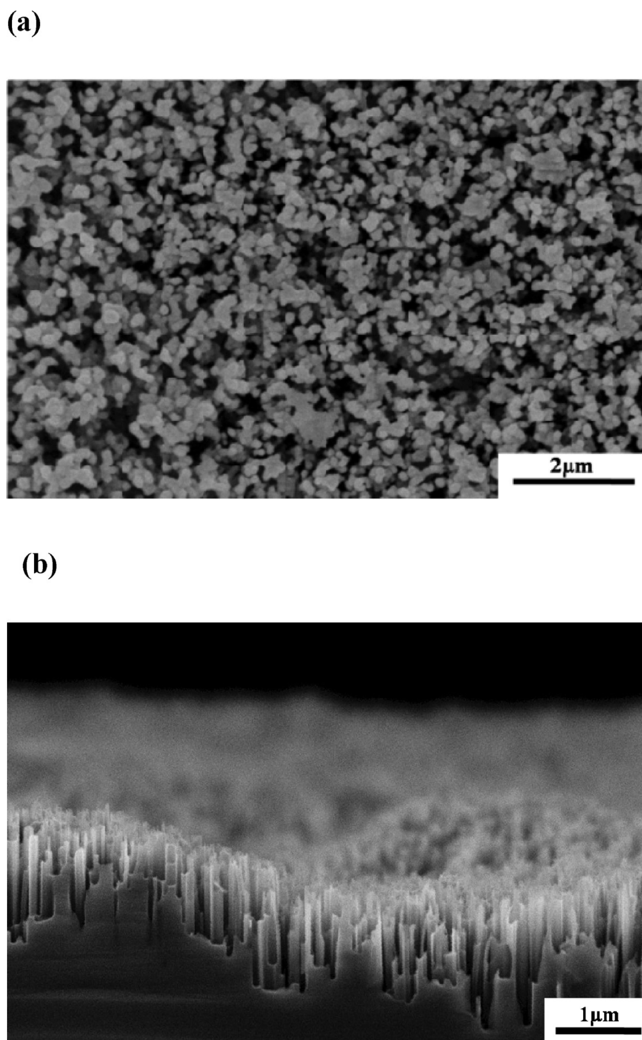

Figure 3. (a) Top-view and (b) cross-sectional SEM images of the SiNW arrays.

wavelength range from 400 to 800 nm (JASCO V-570 UV/Vis/NIR spectrophotometer with integrating sphere). The equivalent oxide charge density (Q_{ox}) and interfacial state density (D_{it}) of the Al_2O_3 layers were extracted using the HP-4284 LCR meter, by performing the high-frequency (100 kHz) capacitance−voltage (C−V) measurement on the $Ni/Al_2O_3/Si$ capacitors at room temperature in an electrically shielded, light-proof probe station. Polished *p*-type Si(100) wafers with resistivity of 1−10 Ω·cm were used as the substrates for the $Ni/Al_2O_3/Si$ capacitors. The ALD and FGA conditions for preparing Al_2O_3 in the $Ni/Al_2O_3/Si$ capacitors were the same as those of the Al_2O_3 surface passivation layer as mentioned above. The Ni top electrode on the $Ni/Al_2O_3/Si$ capacitors was deposited by a thermal evaporator through a shadow mask. The quasi-steady-state photoconductance (QSSPC) technique was used to probe effective minority carrier lifetime using the Sinton WCT-120 lifetime tester. The efficiency of nanotextured black silicon solar cells with an active area of 0.92 cm^2 was examined under the AM 1.5 (100 mW/cm^2 at 25 °C) illumination from a solar simulator. Before the measurement, the light intensity of the solar simulator was calibrated by a standard silicon solar cell. External quantum efficiency (EQE) measurement was carried out at room temperature using the QEX7 solar cell spectral response measurement system.

■ RESULTS AND DISCUSSION

Figure 3 shows the top-view and cross-sectional SEM images of the SiNW array, revealing dense and vertically aligned one-dimensional nanostructures on the surface. The heights of SiNWs are between 0.5 and 1 μm and their diameters are in the range from 30 to 100 nm. The diameters of the SiNWs decrease from bottom to top. Since the diameters and spatial separations of SiNWs are less than the wavelength of sunlight, the SiNW arrays result in strong optical sacttering which can reduce the total reflectance of nanotextured black silicon wafers.

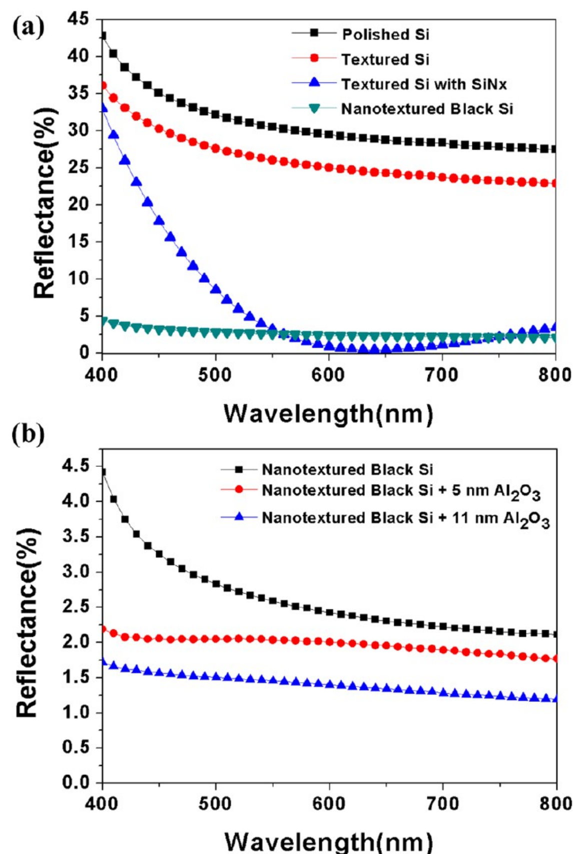

Figure 4. (a) Total reflectance spectra of the polished silicon, texture silicon, texture silicon with a SiN_x AR coating layer, and nanotextured black silicon. (b) Total reflectance spectra of the nanotextured black silicon wafer with and without the Al_2O_3 layers.

Figure 4a shows the total reflectance spectra of the polished silicon, textured silicon, textured silicon with a SiN_x AR coating layer, and nanotextured black silicon wafer, as a function of wavelength from 400 to 800 nm. Significant decrease in the total reflectance of the nanotextured black silicon wafer can be clearly observed in a wide spectral range, as compared with the other samples. The total reflectance of nanotextured black silicon is ∼2.5% in the broad wavelength region from 500 to 800 nm, and slightly increases at the wavelengths less than 500 nm. This low total reflectance of the nanotextured black silicon wafer is ascribed to the morphology of SiNW arrays with subwavelength structure.[5,6,8,10,13,14,30,31] The porosity variation along the vertical direction of the SiNWs leads to a reflective index gradient from bottom to top. Therefore, the SiNW arrays can effectively act as a multilayer AR coating structure and accordingly the nanotextured black silicon wafer exhibited a low total reflectance over a wide spectrum. Figure 4b shows that the total reflectance spectra of the nanotextured black silicon wafers with and without the Al_2O_3 surface passivation layers, indicating that the Al_2O_3 layer further reduces the total reflectance from ∼2.75% (without surface passivation layer) down to ∼2%

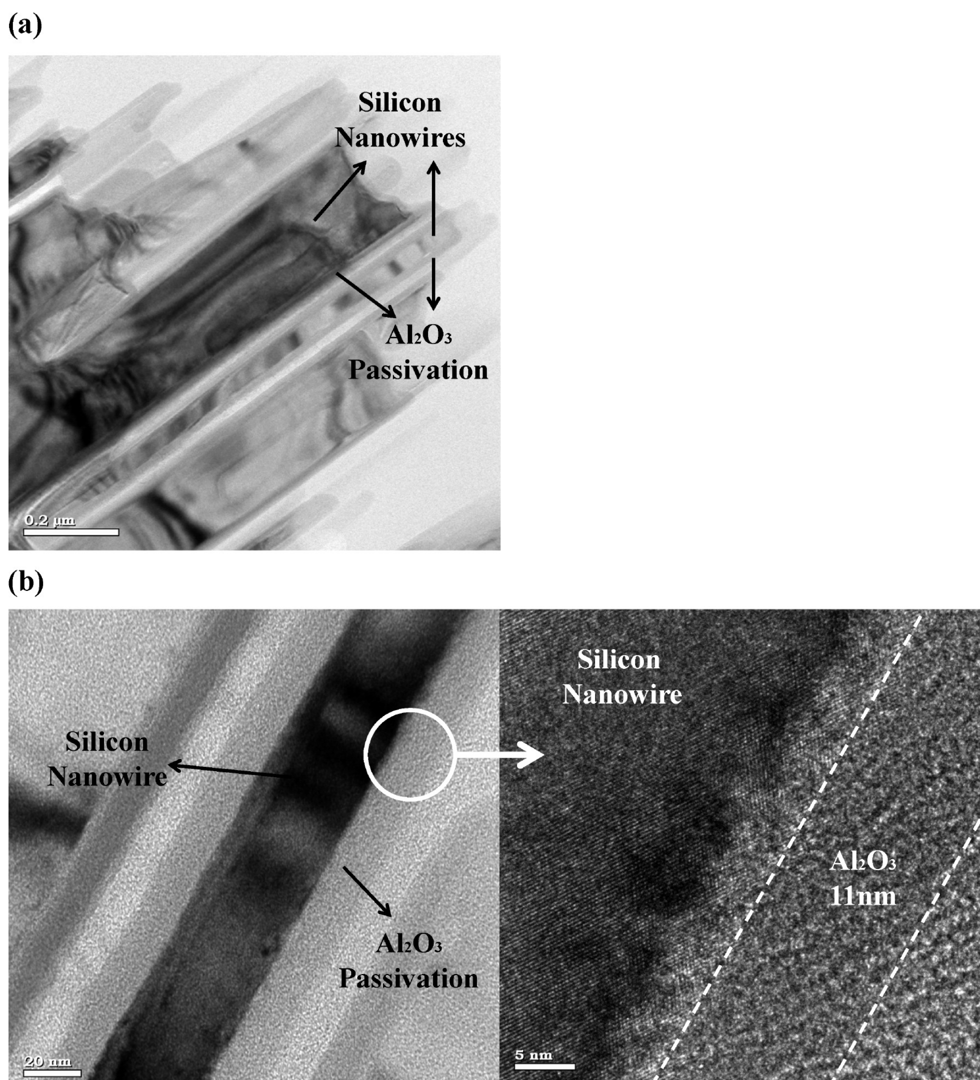

Figure 5. (a) Low-magnification and (b) high-magnification TEM image of the SiNW covered with an Al_2O_3 layer.

(5 nm Al_2O_3) and ∼1.5% (11 nm Al_2O_3). It might be noted that the total reflectance spectra of the nanotextured black silicon wafers covered with the Al_2O_3 layer are almost independent of wavelength in a broad range from 400 to 800 nm, which may be deduced from the gradient in the refractive index profile due to the insertion of a low refractive index layer (Al_2O_3) between the SiNW arrays and air.

Figure 5a,b displays the TEM images of the Al_2O_3 surface passivation layer deposited on the surface of SiNWs. It can be seen from Figure 5b that the thickness of the Al_2O_3 layer is about 11 nm, which is in good agreement with the estimation from the applied 100 ALD cycles. The TEM images also reveal that the SiNW is well-wrapped by the Al_2O_3 layer, demonstrating the good step coverage and high conformality of the thermal ALD technique using the mutiple pulses scheme. Furthermore, the composition distribution of the structure analyzed by EDS is shown in Figure 6, with the scanning region through the nanowrie and the surface passivation layer. The distribution profiles of the elements also suggest the SiNW is surrounded by the Al_2O_3 shell.

Figure 7 shows the normalized $C-V$ characteristics of the $Ni/Al_2O_3/Si$ capacitors, in which the 11 nm Al_2O_3 layer is theoretically ideal ($Q_{ox} = 0$ and $D_{it} = 0$), as-deposited, and treated by FGA before deposition of the Ni top electrode, respectively. Table 1 shows the flat-band voltages V_{fb} determined by the flat-band capacitance C_{fb} in the $C-V$ curves, the Q_{ox} extracted from the shift of V_{fb} with respect to the ideal $C-V$ curve, and the D_{it} calculated by the Terman method. It can be seen that the D_{it} was greatly reduced one order of magnitidue by the FGA treatment, ascribed to the passivation of interfacial states by molecular hydrogen (H_2) contained in the forming gas. The chemical reaction for the hydrogen passivation is given by[32,33]

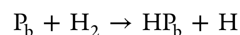

$$P_b + H_2 \rightarrow HP_b + H$$

where P_b represents an unpaired electron localized in a sp^3-like silicon dangling bond at the interface and HP_b denotes the hydrogen-passivated dangling bond. Considerable shift in the $C-V$ curve of the as-deposited Al_2O_3 layer toward the negative voltage direction was clearly observed as compared with that of the ideal Al_2O_3, indicating the presence of net positive Q_{ox} in the as-deposited Al_2O_3 film. The FGA treatment results in a variation of Q_{ox} polarity from positive to negative, as revealed by the positive shift of $C-V$ curve relative to that of the ideal Al_2O_3. The result is in very good agreement with ref 34, which reported the change of the Q_{ox} polarity of the Al_2O_3 thin films

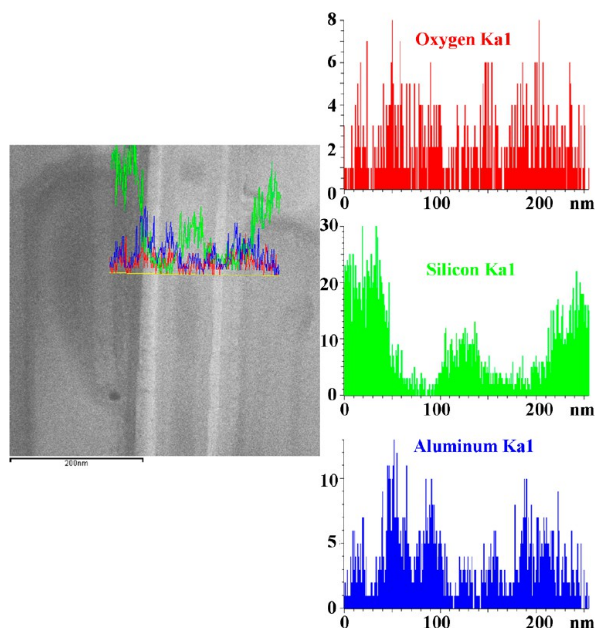

Figure 6. EDS mapping of the element distributions of the SiNW covered with an Al_2O_3 layer. The red, green, and blue lines depict the amounts of oxygen, silicon, and aluminum, respectively.

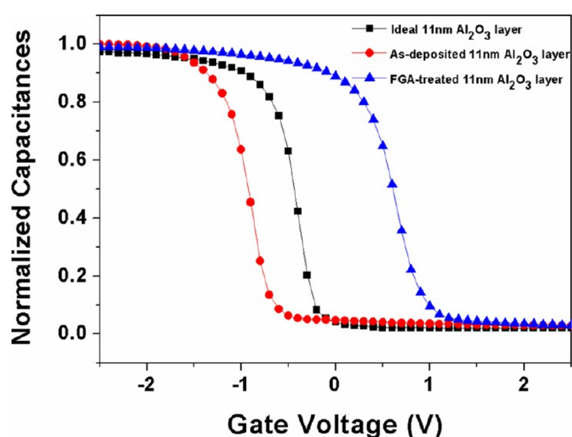

Figure 7. Normalized $C-V$ curves of the $Ni/Al_2O_3/Si$ capacitors, in which the 11 nm Al_2O_3 layer is theoretically ideal, as-deposited, and treated by FGA, respectively.

Table 1. Flat-Band Voltages V_{fb}, Equivalent Oxide Charge Density Q_{ox}, and Interfacial State Density D_{it} of the 11 nm Thick Al_2O_3 Layers Extracted from the $C-V$ Curves Shown in Figure 7

	as-deposited	ideal	FGA-treated
V_{fb} (V)	−0.77	−0.28	0.8
Q_{ox} (cm^{-2})	1×10^{12}	0	-2.6×10^{12}
D_{it} (cm^{-2} eV^{-1})	1.2×10^{12}	0	1.37×10^{11}

treated by the thermal annealing and where the Al_2O_3 films were deposited using the same thermal ALD system (Savannah, Cambridge Nanotech) at identical deposition temperature of 200 °C. The SiO_x interfacial layer between Al_2O_3 and Si should account for the evolution of the Q_{ox} polarity.[20] The negative charge might originate from the tetrahedrally coordinated Al sites at the SiO_x/Al_2O_3 interface.[35] The net negative Q_{ox} in the FGA-treated Al_2O_3 layer might result from the local reconstruction of Al_2O_3 at the SiO_x/Al_2O_3 interface due to the thermal annealing,[34] or the compensation of the positive bulk fixed charge in the Al_2O_3 layer by the FGA treatment.[36]

The origin of the net positive Q_{ox} in the as-deposited Al_2O_3 layer as shown in Figure 7 and Table 1 can be further understood by the $C-V$ characteristucs of the $Ni/Al_2O_3/Si$ capacitors with different Al_2O_3 thickness. Figure 8 shows the

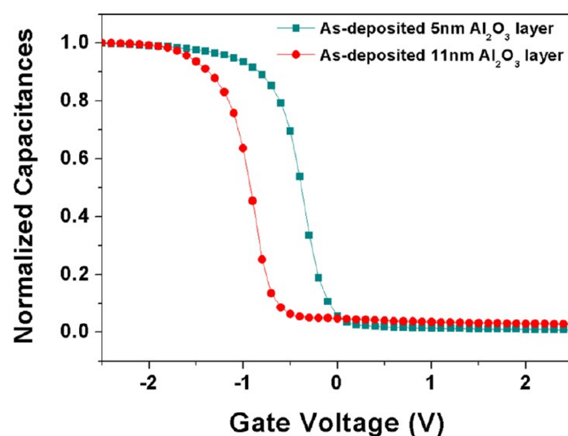

Figure 8. Normalized $C-V$ curves of the $Ni/Al_2O_3/Si$ capacitors, in which the as-deposited Al_2O_3 layer is 5 and 11 nm in thickness, respectively.

normalized $C-V$ curves of the $Ni/Al_2O_3/Si$ capacitors, in which the Al_2O_3 layer is 5 and 11 nm in thickness, respectively, and not treated by FGA. It is seen that the normalized $C-V$ curve of the 5 nm Al_2O_3 layer shifts toward the positive voltage direction in relative to that of the 11 nm Al_2O_3 layer. Table 2

Table 2. Flat-Band Voltages V_{fb}, Equivalent Oxide Charge Density Q_{ox}, and Interfacial State Density D_{it} of the As-Deposited Al_2O_3 Layers with the Thickness of 11 and 5 nm, Respectively, Extracted from the $C-V$ Curves Shown in Figure 8

	11 nm Al_2O_3	5 nm Al_2O_3
V_{fb} (V)	−0.77	-0.2
Q_{ox} (cm^{-2})	1×10^{12}	-4.3×10^{11}
D_{it} (cm^{-2} eV^{-1})	1.20×10^{12}	1.90×10^{12}

displays the V_{fb}, Q_{ox}, and D_{it} of the as-deposited Al_2O_3 layers extracted from the $C-V$ characteristics shown in Figure 8, revealing that the polarity of Q_{ox} turns from positive to negative with the decrease of the film thickness from 11 to 5 nm. This thickness dependence of Q_{ox} can be explained by the presence of the negative fixed charge near the SiO_x/Al_2O_3 interface and the positive bulk fixed charge in Al_2O_3.[36] Accordingly, the polarity of Q_{ox} in the as-deposited Al_2O_3 layers changes from negative to positive as the film thickness increases. The result is consistent with the observation of the thickness dependence of the Q_{ox} polarity of the Al_2O_3 films.[36] It had been reported that the fixed charge is negative at the SiO_x/Al_2O_3 interface, and the defect states in the Al_2O_3 layer are charged positively.[20,36,37] The polarity of the bulk fixed charge in the Al_2O_3 layer is associated with the local stoichiometry, such that the Al-rich regions lead to positive Q_{ox}.[36,38] Therefore, it can be deduced that, as the film thickness increases, the Al-rich regions in the Al_2O_3 layer contribute to greater positive bulk fixed charge than

the negative fixed charge at the SiO_x/Al_2O_3 interface, resulting in the the net positive Q_{ox} in the as-deposited Al_2O_3 layer with the thickness of 11 nm in this study. Table 2 also shows that the D_{it} of 11 nm Al_2O_3 is close to that of 5 nm Al_2O_3, indicating that the interface quality is almost independent of the film thickness.

Figure 9 presents the illuminated current−voltage ($I-V$) curves, and Table 3 shows the open-circuit voltage (V_{oc}), short-circuit current density (J_{sc}), fill-factor (FF), and efficiency (η) of the nanotextured black silicon solar cells, where the Cell-1, -2, and -3 represent the nanotextured black silicon solar cells with and without the 11 nm Al_2O_3 surface passivation layer as well as the post-deposition FGA treatment, respectively. In a comparison of Cell-1 (bare nanotextured black silicon without surface passivation and without FGA) and Cell-2 (with surface passivation but without FGA), one could find that J_{sc} and η were enhanced ∼5.5% and 7.3% by the as-deposited Al_2O_3 surface passivation layer. Thus the efficiency enhancement can be mainly attributed to the increase of J_{sc} due to the suppression of surface recombination by the as-deposited Al_2O_3 passivation layer and the improvement in light coupling as shown in Figure 4b. As compared with Cell-2, a further increase of V_{oc}, J_{sc}, FF, and η was observed in Cell-3 (with surface passivation and with FGA) as a result of the significant suppression of D_{it} by the FGA treatment as revealed in Figure 7 and Table 1. Thus a high efficiency of 18.2% was achieved in Cell-3, as shown in Figure 9b. A comparison of Cell-3 with Cell-1 indicates a 8% increment of J_{sc} and 10.3% increment of η by the ALD Al_2O_3 surface passivation layer together with the FGA treatment.

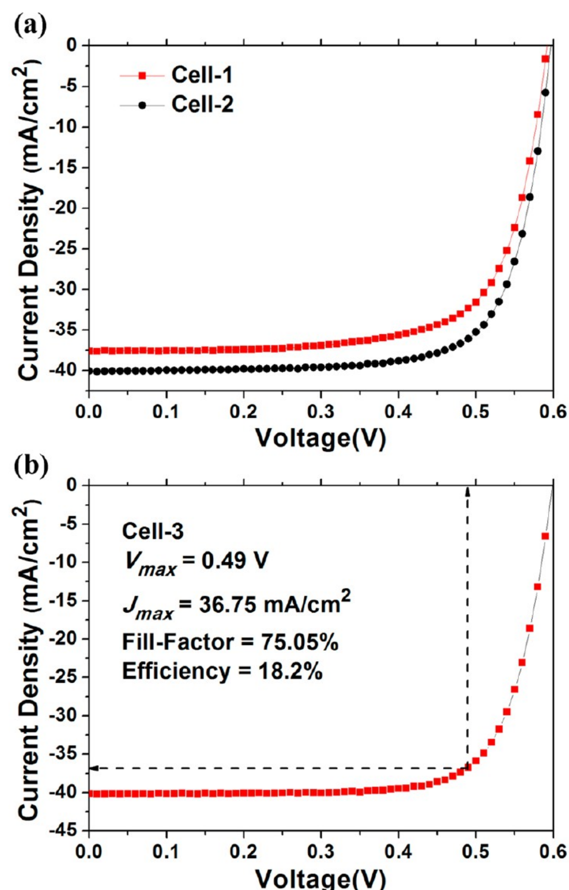

Figure 9. Illuminated $I-V$ characteristics of the (a) Cell-1 and -2 and (b) Cell-3.

Table 3. Open Circuit Voltage (V_{oc}), Short-Circuit Current Density (J_{sc}), Fill-Factor (FF), and Efficiency (η) of the Nanotextured Black Silicon Solar Cells[a]

	V_{oc} (V)	J_{sc} (mA/cm^2)	FF (%)	η (%)
Cell-1	0.589	37.93	73.17	16.5
Cell-2	0.590	40.03	74.08	17.7
Cell-3	0.598	41.26	75.05	18.2

[a]Cell-1: without surface passivation and without FGA. Cell-2: with the 11 nm Al_2O_3 passivation layer but without FGA. Cell-3: with the 11 nm Al_2O_3 passivation layer and with FGA.

The effect of surface passivation was further examined by the QSSPC and EQE measurements. Table 4 displays the implied one-sun open-circuit voltage (V_{oc}) and effective minority carrier lifetime (τ) of the nanotextured black silicon wafers associated with Cell-1, -2, and -3, respectively. As compared with the nanotextured black silicon without the surface passivation (Cell-1), the effective lifetime τ of the sample covered by the as-deposited Al_2O_3 passivation layer (Cell-2) increases by one order of magnitude from 1.05 to 12.8 μs, and the implied V_{oc} also increases from 520 to 573 mV. After the FGA treatment, the implied V_{oc} and effective lifetime τ further increases to 583 mV and 18.1 μs. Figure 10 shows the EQE of the Cell-1, -2, and -3 as a function of wavelength from 300 to 1100 nm. Both Cell-2 and -3 exhibited greater EQE almost across a full spectral range from ∼300 to 1000 nm than Cell-1, which could be attributed to the suppressed surface recombination together with the further reduced total reflectance over a broad spectrum by the Al_2O_3 passivation layer as shown in Figure 4b. The low

Table 4. Implied One-Sun V_{oc} and Effective Minority Carrier Lifetime τ of the Nanotextured Black Silicon Wafers Associated with Cell-1, -2, and -3

sample	implied one-sun open-circuit voltage (mV)	effective minority carrier lifetime (μs)
Cell-1	520	1.05
Cell-2	573	12.8
Cell-3	583	18.1

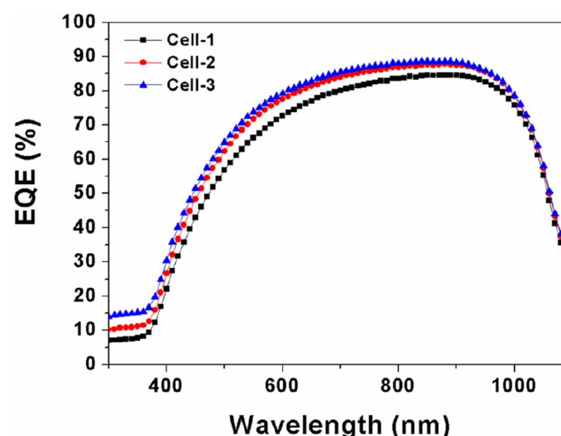

Figure 10. EQE as a function of wavelength of the Cell-1, -2, and -3.

EQE at short wavelengths results from the loss of surface recombination due to a great amount of defects created by the fabrication process of SiNWs. The ALD Al_2O_3 surface passivation and FGA treatment indeed increase the EQE near $\lambda \sim 400$ nm; however, the improvement is marginal as compared with the increment of EQE between 500−900 nm. As shown in Table 1, the net positive Q_{ox} in the as-deposited Al_2O_3 layer is appropriate for the surface passivation on the n^+ emitter; however, the D_{it} of the as-deposited Al_2O_3 film is not low enough. As for the FGA-treated Al_2O_3 layer, the reduced D_{it} is beneficial to chemical passivation but the net negative Q_{ox} is detrimental to field-effect passivation. Thus the limited increment of EQE at short wavelengths can be ascribed to the high D_{it} of the as-deposited Al_2O_3 film and the inappropriate negative Q_{ox} in the FGA-treated Al_2O_3 layer, respectively. However, the greater improvement in EQE and longer minority carrier lifetime of the FGA-treated layer than the as-deposited film, as shown in Figure 10 and Table 4, suggest that the chemical passivation based on the reduction in D_{it} is more effective than the field-effect passivation built by the appropriate Q_{ox}. A surface passivation layer with low D_{it}, positive Q_{ox}, and high conformality is desired on the nanotextured black silicon solar cells with the n^+ emitter/ p- base structure, which needed to be further developed.

As compared with the nanotextured black silicon solar cells reported in ref 14, another reason for the high efficiency in this study might come from the improvement of FF. The poor Ohmic contact as a result of the granular morphology of the metal electrodes is another reason to explain the lower efficiency of nanotextured black silicon solar cells than conventional textured silicon solar cells.[12,14,39] Figure 11 shows the cross-sectional SEM images of the Ni/Ag metal contact upon the SiNW arrays, revealing that the Ni/Ag electrode is a smooth and continuous film prepared by thermal evaporation. This smooth and continuous electrode may be beneficial to the increase in FF of the nanotextured black slicon solar cells.

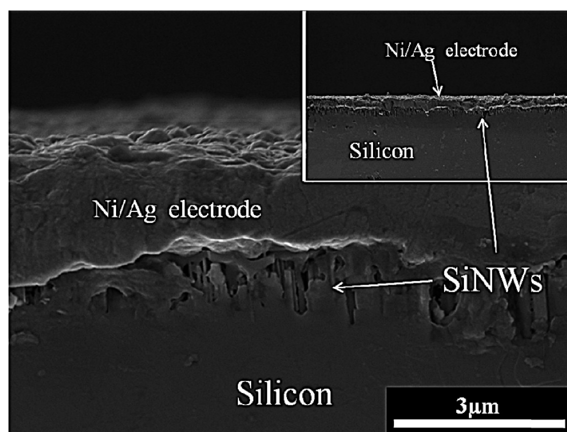

Figure 11. Cross-sectional SEM image of the Ni/Ag electrode upon the SiNW arrays.

■ CONCLUSIONS

Efficient (18.2%) nanotextured black silicon solar cells with the ALD Al_2O_3 surface passivation and the n^+ emitter/p base structure were demonstrated. Silver-catalyzed wet chemical etching was used to fabricate the SiNW arrays on the n^+ emitter of the nanotextured black silicon solar cells, to offer the broadband and omnidirectional antireflection. The thermal ALD technique using the multiple pulses scheme was utilized to deposit the conformal Al_2O_3 layer upon the surface of the SiNWs, so as to reduce the surface recombination and the total reflectance. The nanotextured black silicon wafer covered with the 11 nm Al_2O_3 layer exhibited a low total reflectance of ~1.5% in a wide spectral range from 400 to 800 nm. The effective minority carrier lifetime in the nanotextured black silicon was significantly increased with one order of magnitude by the Al_2O_3 passivation layer due to the suppressed surface recombination. As compared with the bare nanotextured black silicon solar cells, the ALD Al_2O_3 surface passivation layer coupled with the FGA treatment leads to 8% increment of short-circuit current density and 10.3% enhancement of efficiency. The modified device structure for increasing the fill factor, the improved morphology of the SiNW arrays for broadening the antireflection, and other surface passivation materials with low D_{it}, appropriate Q_{ox}, and high conformality for further reducing surface recombination will be developed to enhance the performance of nanotextured black silicon solar cells in the future.

■ AUTHOR INFORMATION

Corresponding Author

*E-mail: mjchen@ntu.edu.tw.

Notes

The authors declare no competing financial interest.

■ REFERENCES

(1) Zhao, J.; Wang, A.; Green, M. A.; Ferrazza, F. *Appl. Phys. Lett.* **1991**, *73*, 1991−1993.
(2) Inomata, Y.; Fukui, K.; Shirasawa, K. *Sol. Energy Mater. Sol. Cells* **1997**, *48*, 237−242.
(3) Otto, M.; Kroll, M.; Käsebier, T.; Lee, S.-M.; Putkonen, M.; Salzer, R.; Miclea, P. T.; Wehrspohn, R. B. *Appl. Phys. Lett.* **2012**, *100*, 191603.
(4) Jansen, H.; Boer, M.D.; Legtenberg, R.; Elwenspoek, M. *J. Micromech. Microeng.* **1995**, *5*, 115−120.
(5) Huang, Y. F.; Chattopadhyay, S.; Jen, Y. H.; Peng, C. Y.; Liu, T. A.; Hsu, Y. K.; Pan, C. L.; Lo, H. C.; Hsu, C. H.; Chang, Y. H.; Lee, C. S.; Chen, K. H.; Chen, L. C. *Nat. Nanotechnol.* **2007**, *2*, 770−774.
(6) Yuan, H.C.; Yost, V. E.; Page, M. R.; Stradins, P.; Meier, D. L.; Branz, H. M. *Appl. Phys. Lett.* **2009**, *95*, 123501.
(7) Fang, H.; Wu, Y.; Zhao, J. H.; Zhu, J. *Nanotechnology* **2006**, *17*, 3768−3774.
(8) Srivastava, S. K.; Kumar, D.; Singh, P. K.; Kar, M.; Hussain, M.; Kumar, V. *Sol. Energy Mater. Sol. Cells* **2010**, *94*, 1506−1511.
(9) Sai, H.; Fujii, H.; Arafune, K.; Ohshita, Y.; Kanamori, Y.; Yugami, H.; Yamaguchiy, M. *Jpn. J. Appl. Phys.* **2007**, *46*, 3333−3336.
(10) Lu, Y.T.; Barron, A. R. *Chem. Chem. Phys.* **2013**, *15*, 9862−9870.
(11) Bilyalov, R.R.; Stalmans, L.; Schirone, L.; Lévy-Clément, C. *IEEE Trans. Electron Devices* **1999**, *46*, 2035−2040.
(12) Stalmans, L.; Poortmans, J.; Bender, H.; Caymax, M.; Said, K.; Vazsonyi, E.; Nijs, J.; Mertens, R. *Prog. Photovoltaics: Res. Appl.* **1998**, *6*, 233−246.
(13) Peng, K.; Xu, Y.; Wu, Y.; Yan, Y.; Lee, S. T.; Zhu, J. *Small* **2005**, *1*, 1062−1067.
(14) Kumar, D.; Srivastsva, S.K.; Singh, P.K.; Husain, M.; Kumar, V. *Sol. Energy Mater. Sol. Cells* **2011**, *95*, 215−218.
(15) Chen, M. J.; Shih, Y. T.; Wu, M. K.; Tsai, F. Y. *J. Appl. Phys.* **2007**, *101*, 033130.
(16) Aberle, A. G. *Prog. Photovoltaics: Res. Appl.* **2000**, *8*, 473−487.
(17) Oh, J.; Yuan, H. C.; Branz, H. M. *Nat. Nanotechnol.* **2012**, *7*, 743−748.

(18) Mariani, G.; Scofield, A. C.; Hung, C. H.; Huffaker, D. L. *Nat. Commun.* **2013**, *4*, 1497.
(19) Holm, J. V.; Jørgensen, H. I.; Krogstrup, P.; Nygård, J.; Liu, H.; Aagesen, M. *Nat. Commun.* **2013**, *4*, 1498.
(20) Hoex, B.; Gielis, J. J. H.; van de Sanden, M. C. M.; Kessels, W. M. M. *J. Appl. Phys.* **2008**, *104*, 113703.
(21) Agostinelli, G.; Delabie, A.; Vitanov, P.; Alexieva, Z.; Dekkers, H. F. W.; Wolf, S. De.; Beaucarne, G. *Sol. Energy Mater. Sol. Cells* **2006**, *90*, 3438−3443.
(22) Dingemans, G.; Kessels, W. M. M. *J. Vac. Sci. Technol. A* **2012**, *30*, 040802.
(23) Repo, P.; Haarahiltunen, A.; Sainiemi, L.; Marko, Y.K.; Talvitie, H.; Schubert, M. C.; Savin, H. *IEEE J. Photovoltaics* **2013**, *3*, 90−94.
(24) Researchers at Fraunhofer ISE of Germany and Aalto University of Finland have developed a black silicon solar cell that achieved 18.7% efficiency. http://cleantechnica.com/2013/04/05/black-silicon-solar-cell-efficiency-record-broken/ (accessed 2013).
(25) Benick, J.; Hoex, B.; van de Sanden, M. C. M.; Kessels, W. M. M.; Schultz, O.; Glunz, S. *Appl. Phys. Lett.* **2008**, *92*, 253504.
(26) Schmidt, J.; Merkle, A.; Brendel, R.; Hoex, B.; van de Sanden, M. C. M.; Kessels, W. M. M. *Prog. Photovoltaics: Res. Appl.* **2008**, *16*, 461−466.
(27) Profijt, H. B.; Potts, S. E.; van de Sanden, M. C. M.; Kessels, W. M. M. *J. Vac. Sci. Technol.* **2011**, *29*, 050801.
(28) Kumar, D.; Srivastava, S.K.; Singh, P.K.; Sood, K.N.; Singh, V.N.; Dilawar, N.; Husain, M. *J. Nanopart. Res.* **2010**, *12*, 2267−2276.
(29) Elam, J. W.; Libera, J. A.; Pellin, M. J. *Appl. Phys. Lett.* **2007**, *91*, 243105.
(30) Kanamori, Y.; Sasaki, M.; Hane, K. *Opt. Lett.* **1999**, *24*, 1422−1424.
(31) Chao, Y. C.; Chen, C. Y.; Lin, C. A.; He, J. H. *Energy Environ. Sci.* **2011**, *4*, 3436−3441.
(32) Brower, K. L.; Myers, S. M. *Appl. Phys. Lett.* **1990**, *57*, 162−164.
(33) Cartier, E.; Stathis, J. H.; Buchanan, D. A. *Appl. Phys. Lett.* **1993**, *63*, 1510−1512.
(34) Lei, D.; Yu, X.; Song, L.; Gu, X.; Li, G.; Yang, D. *Appl. Phys. Lett.* **2011**, *99*, 052103.
(35) Johnson, R. S.; Lucovsky, G.; Baumvol, I. *J. Vac. Sci. Technol.* **2001**, *19*, 1353−1360.
(36) Shin, B.; Weber, J. R.; Long, R. D.; Hurley, P. K.; Van de Walle, C. G.; et al. *Appl. Phys. Lett.* **2010**, *96*, 152908.
(37) Ahn, Y.; Choudhury, S. H.; Lee, D.; Sadaf, S. M.; Siddik, M.; Jo, M.; Park, S.; Kim, Y. D.; Kim, D. H.; Hwang, H. *Jpn. J. Appl. Phys.* **2011**, *50*, 071503.
(38) Weber, J. R.; Janotti, A.; Van de Walle, C. G. *J. Appl. Phys.* **2011**, *109*, 033715.
(39) Fang, H.; Li, X.; Song, S.; Xu, Y.; Zhu, J. *Nanotechnology* **2008**, *19*, 1−6.